ACS APPLIED MATERIALS & INTERFACES

Research Article

www.acsami.org

Various Bismuth Oxyiodide Hierarchical Architectures: Alcohothermal-Controlled Synthesis, Photocatalytic Activities, and Adsorption Capabilities for Phosphate in Water

Quan-Cheng Liu, De-Kun Ma,* Ying-Ying Hu, Ya-Wen Zeng, and Shao-Ming Huang*

Nanomaterials and Chemistry Key Laboratory, Wenzhou University, Wenzhou, Zhejiang 325027, People's Republic of China

Supporting Information

ABSTRACT: Controllable synthesis of morphology and composition of functional material through a similar method is very necessary to understand the related properties. In this study, we report a facile solvothermal route to synthesize a series of bismuth oxyiodide compounds, including BiOI, $Bi_7O_9I_3$, and $Bi_4O_5I_2$ hierarchical microspheres, under relatively mild conditions through only adjusting the types of alcohols. It was found that the viscosity of alcohol played key roles in determining the morphologies and compositions of the final products. UV−visible diffuse-reflectance spectra and theoretic calculations indicated that bismuth oxyiodides with different ratios of Bi:O:I clearly possessed different light absorption and energy band structures. As a result, the as-synthesized BiOI, $Bi_7O_9I_3$, and $Bi_4O_5I_2$ hierarchical microspheres displayed morphology- and composition-dependent photocatalytic activities for the degradation of rhodamine B (RhB) and colorless phenol under visible-light irradiation. On the basis of experimental results, the difference of photocatalytic activity of these bismuth oxyiodide compounds was discussed. Furthermore, hierarchical bismuth oxyiodide microspheres were also evaluated as adsorbents for removing phosphate from aqueous solution. The results showed that $Bi_7O_9I_3$ and $Bi_4O_5I_2$ hierarchical microspheres had good adsorption capabilities for phosphate in water because of their larger surface areas and hierarchical porous structures.

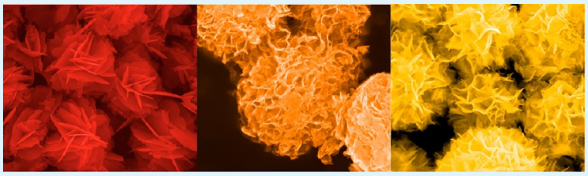

KEYWORDS: *bismuth oxyiodides, hierarchical architecture, alcohothermal synthesis, photocatalytic activity, adsorption capability*

1. INTRODUCTION

With the increasingly serious environmental problems, environmentally benign syntheses of functional materials and green environmental treatment techniques have attracted much attention.[1−5] Among various known alcohols, ethanol, ethylene glycol, and glycerol have negligible toxicity. However, compared with water, they are seldom used as solvents to synthesize various functional materials with a well-defined morphology and composition.[6−8] On the other hand, photocatalysis can utilize sunlight and remove pollutants in water and air, which has been considered as a kind of green and efficient technique to purify the environment.[9] Adsorption is also one of the most effective and economical technologies to remove pollutants.[10] Recently, hierarchical architectures fabricated by nanounits, such as nanoparticles, nanorods, and nanosheets, have exhibited promising applications in the field of environmental remediation.[11−15] Photocatalysts with hierarchical architectures possess many advantages: (1) keeping as high as photocatalytic activity of nanounits; (2) facilitating the transportation of reactants to the surfaces of the photocatalysts because of the abundant interspaces formed among adjacent nanounits; (3) capturing more light energy because of multireflection of light on the surfaces of neighboring nanounits; (4) easily separated and recycled as the total size of the hierarchical architecture is in micrometer scale; and (5) displaying special wettability in some cases, which will benefit some specific photocatalytic reaction system. As far as adsorbents with hierarchical architectures are concerned, they hold high specific surface areas and accessible diffusion pathways and thus exhibit excellent adsorption capacity for removing contaminants.[16] Up to now, there have been many successful methodologies for the fabrication of hierarchical architectures, such as self-assembly,[17] oriented aggregation of nanounits,[18] templating synthesis,[19] sequential nucleation and growth,[20] self-construction of the crystals, and topochemical conversion.[21,22] Comparatively speaking, direct self-assembly of nanounits is the simplest method for constructing hierarchical architectures among them. Considering the above facts, it is very necessary to develop a new alcohothermal route to synthesize various hierarchical architectures through direct self-assembly for the purpose of environmental treatment.

Bismuth oxyiodides belong to main group V−VI−VII ternary semiconductors with layered crystal structures. In the structures, positive $Bi_xO_y^{n+}$ slabs are interleaved with anionic iodide slabs and the resulting internal static electric fields are perpendicular to each layer. The inherent electric fields were believed to facilitate the separation of photogenerated electrons and holes.[23] As a result, bismuth oxyiodide compounds were

Received: August 29, 2013
Accepted: October 18, 2013
Published: October 18, 2013

   dx.doi.org/10.1021/am4036702 | ACS Appl. Mater. Interfaces 2013, 5, 11927−11934

expected to demonstrate good photocatalytic activity. Up to now, five different bismuth oxyiodide compounds, including BiOI, $Bi_4O_5I_2$, α-Bi_5O_7I, β-Bi_5O_7I, and $Bi_7O_9I_3$, have been reported.[24] Among them, BiOI has been widely studied as photocatalysts.[25−28] However, the study of morphology- and composition-controlled syntheses and applications for the other oxygen-rich bismuth oxyiodide compounds is still at their preliminary stages.[29]

Herein, we develop a facile alcohothermal route to synthesize BiOI, $Bi_4O_5I_2$, and $Bi_7O_9I_3$ hierarchical microspheres assembled by nanosheets, using ethanol, ethylene glycol, and glycerol as solvents, respectively. The formation mechanisms of bismuth oxyiodide hierarchical architectures were proposed on the basis of experimental results. The optical absorption, energy band structures, and photocatalytic activities for the degradation of dye RhB and colorless phenol under visible-light irradiation of the products were comparatively studied. In addition, the adsorption capabilities of these hierarchical bismuth oxyiodides for phosphate in water were also surveyed.

2. EXPERIMENTAL SECTION

2.1. Synthesis of Bismuth Oxyiodide Hierarchical Architectures. All chemical reagents were purchased from Aladdin and used as received. All the synthetic processes of BiOI, $Bi_4O_5I_2$, and $Bi_7O_9I_3$ hierarchical microspheres are similar except for the types of alcohols used. In a typical procedure for the synthesis of $Bi_4O_5I_2$, 0.8 mmol of $Bi(NO_3)_3{\cdot}5H_2O$ was dissolved into 38 mL of glycerol under vigorous stirring. Then 0.8 mmol of NaI was put into 2 mL of ultrapure water, and the solution was continuously agitating until the aqueous solution became clear. After that, the solution was slowly added into the above glycerol solution containing $Bi(NO_3)_3{\cdot}5H_2O$ under stirring. Subsequently, the solution was put into a Teflon-lined stainless steel autoclave with a capacity of 60 mL and heated at 130 °C for 12 h. After the autoclave was cooled to room temperature, the products were separated centrifugally and washed three times with ultrapure water and absolute ethanol. Finally, the products were dried under vacuum at 60 °C for 4 h.

2.2. Characterization. Powder X-ray diffraction (XRD) patterns were carried out on a Bruker D8 Advanced X-ray diffractometer using Cu Kα radiation (λ = 0.15418 nm) at a scanning rate of 8°/min in the 2θ range of 10−70°. Field emission scanning electron microscopy (FE-SEM) images were taken on a Nova NanoSEM 200 scanning electron microscope. Transmission electron microscopy (TEM) images, high-resolution transmission electron microscopy (HRTEM) images, and energy-dispersive X-ray (EDX) spectra were taken on a JEOL 2010 microscope, using an accelerating voltage of 200 kV. The UV−visible diffuse-reflectance spectra (UV−vis DRS) were recorded on a UV2450 (Shimadzu) using $BaSO_4$ as reference. The Brunauer−Emmett−Teller (BET) surface area was measured with an ASAP2020 specific surface area and porosity analyzer.

2.3. Photocatalytic Properties. Photocatalytic activities of hierarchical bismuth oxyiodide compounds were evaluated by the degradation of RhB and phenol in water under visible-light irradiation from a 500 W Xe lamp (CHF-XM500, purchased from Beijing Changtuo Science and Technology Co. Ltd.) equipped with a 400 nm cutoff filter. For the degradation of RhB, in every experiment, 100 mg of the photocatalysts was added to 100 mL of RhB solution (5×10^{-5} mol/L). Before illumination, the suspensions were magnetically stirred in the dark for 8 h to ensure the establishment of an adsorption−desorption equilibrium between the photocatalysts and the dye. After that, the solution was exposed to visible-light irradiation under magnetic stirring. At given time intervals, 3 mL aliquots were sampled and centrifuged to remove the photocatalyst particles. Then, the filtrates were analyzed by recording variations of the absorption band maximum (553 nm) in the UV−visible spectra of the dye by using a Shimadzu UV2450 PC spectrophotometer. As to photocatalytic degradation of phenol, keeping other conditions unchanged, the initial concentration of the phenol solution was 1×10^{-4} mol/L. After visible-light irradiation for different periods of time, the centrifugated solution was analyzed by recording variations of the absorption band maximum (270 nm) of phenol in the UV−vis spectra by using a Shimadzu UV2450 PC spectrophotometer.

2.4. Phosphate Adsorption Experiments. A 100 mg portion of the samples was added into a flask filled with 500 mL of phosphate solution (10 mg/L). The pH value of the solution was kept at 7.0 by using NaOH or HCl solutions. After stirring for a certain time at room temperature, 10 mL aliquots were sampled and centrifuged to remove the adsorbents. Phosphate concentrations in the solutions were determined by the molybdenum blue method through monitoring the absorbance at 700 nm on a UV−vis spectrophotometer.[16]

3. RESULTS AND DISCUSSION

3.1. XRD Characterizations. Figure 1 represents XRD patterns of the products synthesized with different alcohols. As

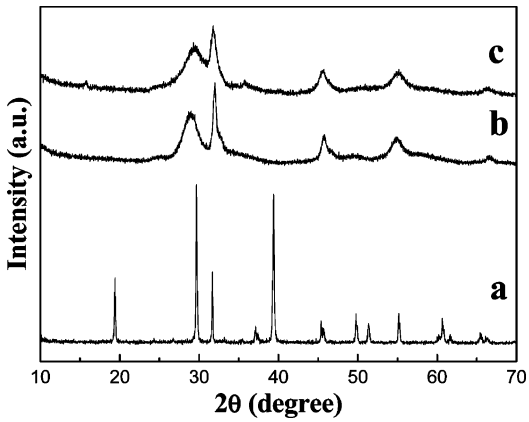

Figure 1. XRD patterns of the products synthesized with different solvents: ethanol (a), ethylene glycol (b), and glycerol (c).

shown in Figure 1, pattern a, using ethanol as solvent, the resultant products are pure BiOI. All of the diffraction peaks in Figure 1, pattern a, can be well-indexed to tetragonal phase BiOI (JCPDS no. 73-2062). No other obvious impurities can be detected. Interestingly, selecting ethylene glycol and glycerol as solvents, the final products become $Bi_7O_9I_3$ (Figure 1, pattern b) and $Bi_4O_5I_2$ (Figure 1, pattern c), respectively. The positions of diffraction peaks of the products are in agreement with previous reports on $Bi_7O_9I_3$ and $Bi_4O_5I_2$.[29,30] Compared with the as-synthesized BiOI, the diffraction peaks of the as-obtained $Bi_7O_9I_3$ and $Bi_4O_5I_2$ obviously widen, suggesting that the latter products have smaller crystal units. In addition, the characteristic diffraction peaks of $Bi_7O_9I_3$ and $Bi_4O_5I_2$, respectively, located at 28.7° and 29.5° obviously shift to smaller diffraction angles compared that of standard BiOI, which can be ascribed to the extra oxygen and bismuth in the lattice of BiOI, thus causing its expansion and structural distortion.[24]

3.2. Microscopy Observations. The morphology of the samples was observed by FE-SEM. As shown in Figure 2a, the sample BiOI takes on flower-like hierarchical architectures, which are constructed by many straight nanosheets. Unlike BiOI, the $Bi_7O_9I_3$ sample is a hierarchical microsphere assembled by many bent nanosheets (Figure 2b). The morphology of $Bi_4O_5I_2$ is similar to that of $Bi_7O_9I_3$, but its diameter is clearly smaller than the latter. The morphologies of the samples were further surveyed by TEM. Consistent with FE-SEM observations, TEM images also show that the present

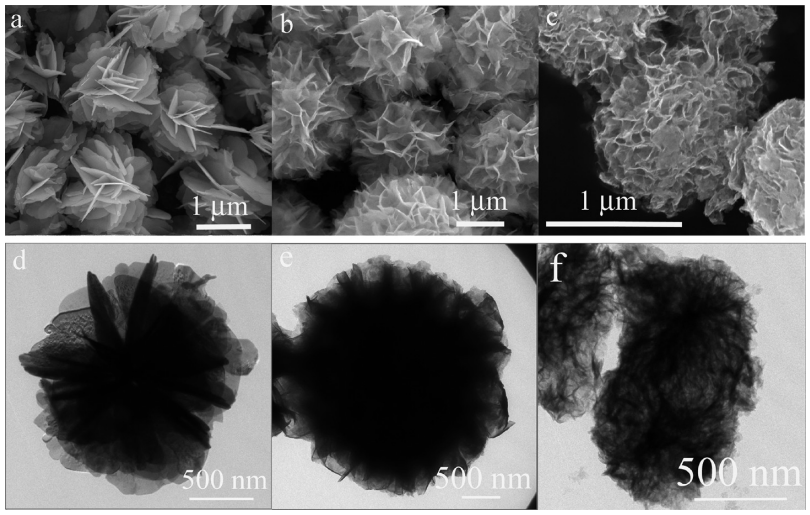

Figure 2. FE-SEM images of the as-synthesized BiOI (a), $Bi_7O_9I_3$ (b), and $Bi_4O_5I_2$ (c) and the corresponding TEM images: BiOI (d), $Bi_7O_9I_3$ (e), and $Bi_4O_5I_2$ (f).

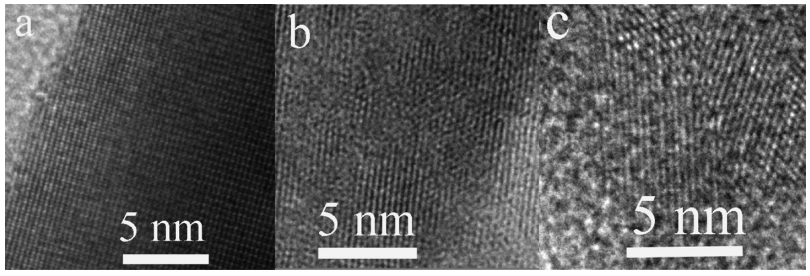

Figure 3. HRTEM images performed on the rims of nanosheets for fabricating hierarchical BiOI (a), $Bi_7O_9I_3$ (b), and $Bi_4O_5I_2$ (c) microspheres.

bismuth oxyiodide compounds possess hierarchical architectures fabricated by nanosheets. However, combined with FE-SEM observations, it can be seen from TEM images that the thicknesses of nanosheets gradually decrease from BiOI through $Bi_7O_9I_3$ to $Bi_4O_5I_2$. The result is also consistent with the above XRD analysis.

The elaborate structures and compositions of hierarchical BiOI, $Bi_7O_9I_3$, and $Bi_4O_5I_2$ were identified by HRTEM images and EDX spectra. All HRTEM images were recorded on the rims of nanosheets that were nanounits for constructing corresponding hierarchical microspheres. As shown in Figure 3a–c, these bismuth oxyiodide nanosheets display clear lattice fringes, suggesting that they possess good crystallinity, which is very beneficial to their photocatalytic activity. The corresponding EDX spectra recorded on individual microspheres of BiOI, $Bi_7O_9I_3$, and $Bi_4O_5I_2$ show that all of the samples consist of Bi, O, I, C, and Cu elements (Supporting Information, Figure S1). The existence of C and Cu chiefly originates from the carbon-coated copper grid, which is usually used as the samples' supporter. The results show that the as-obtained products are bismuth oxyiodides. The calculated ratios of Bi:O:I in the samples synthesized with ethanol, ethylene glycol, and glycerol are 1:1.1:1, 1:1.3:0.44, and 1:1.18:0.48, respectively, which are near to theoretic ratios of Bi:O:I in BiOI, $Bi_7O_9I_3$, and $Bi_4O_5I_2$. Combined with all the above results, it can be definitely concluded that BiOI, $Bi_7O_9I_3$, and $Bi_4O_5I_2$ with various hierarchical architectures have been achieved through the alcohothermal route presented here.

3.3. Formation Mechanism of Hierarchical Bismuth Oxyiodides. For the syntheses of BiOI, $Bi_7O_9I_3$, and $Bi_4O_5I_2$ hierarchical microspheres, all of the conditions are the same except for the use of different alcohols. Therefore, the differences of physical and chemical properties of alcohols undoubtedly played crucial roles in determining the morphologies and compositions of the final products. In the experimental process, it was observed that plenty of precipitates were produced after NaI was added into the ethanol reaction system and only stirred for several minutes, whereas no precipitates occurred for ethylene glycol and glycerol systems during the whole stirring process. After reacting in the autoclave for 1 h, solid products were observed in the ethylene glycol system, whereas the formation of solid products needed ca. 3 h for the glycerol system. The above phenomena indicate that the types of alcohols largely affect the chemical reaction rates of bismuth oxyiodides. For the solution phase reaction, reactant molecules in solvent need to meet and collide with other reactant molecules through the diffusion mode. According to the Stokes–Einstein equation, $D = kT/6\pi\eta r$, where D represents the diffusion coefficient, k is the Boltzmann constant, T is the absolute temperature, η is the viscosity of solvent, and r is the radius of the reaction molecule; D is inversely proportional to η when the other conditions are kept unchanged. The viscosity of ethanol, ethylene glycol, and glycerol is 1.07, 26.09, and 934 $mN{\cdot}s{\cdot}m^{-2}$ at room temperature, respectively. Therefore, ethanol has the largest diffusion rate among them when it was used as the medium. Selecting ethylene glycol and glycerol as solvents, the corresponding reactions have a smaller diffusion rate, which determines the whole chemical reaction rates. As a result, both the formations of $Bi_7O_9I_3$ and $Bi_4O_5I_2$ hierarchical microspheres were

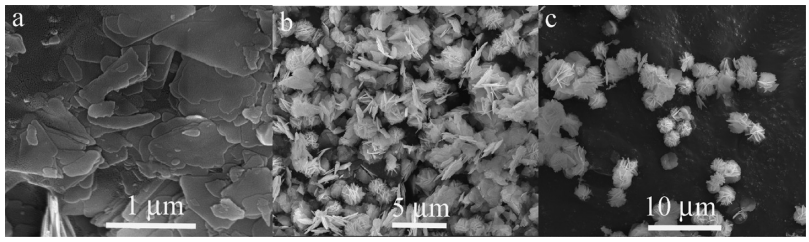

Figure 4. FE-SEM images of the samples obtained at different reaction times: (a) 0, (b) 2, and (c) 4 h.

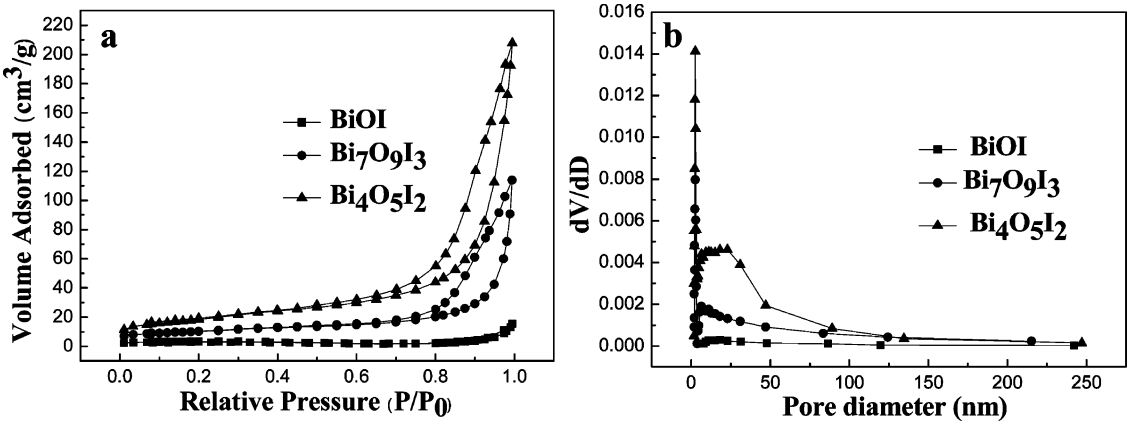

Figure 5. Nitrogen adsorption and desorption isotherms (a) and pore size distribution curves (b) of BiOI, $Bi_7O_9I_3$, and $Bi_4O_5I_2$ hierarchical microspheres.

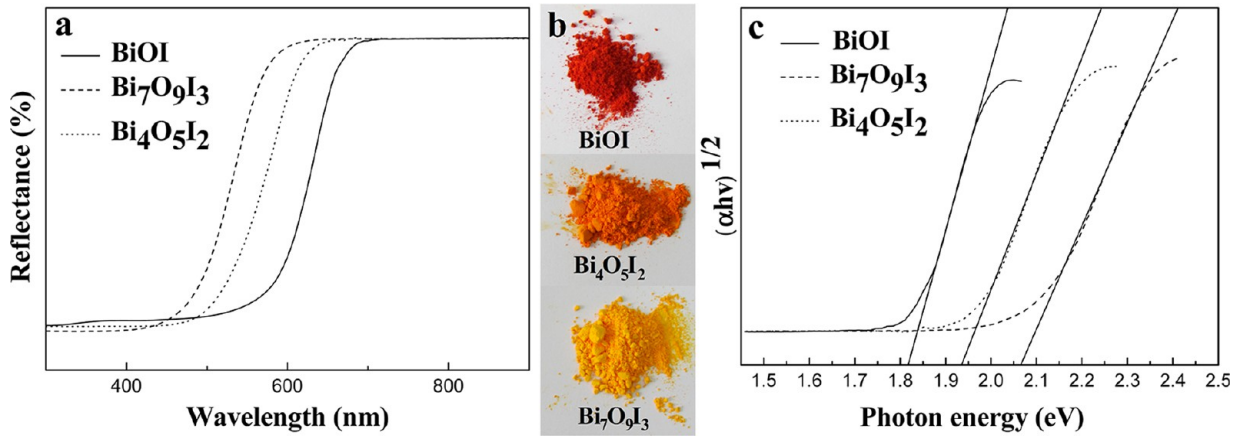

Figure 6. UV−vis DRS spectra (a), digital photos (b), and plots of $(\alpha h\nu)^{1/2}$ versus the photon energy ($h\nu$) (c) of the as-synthesized BiOI, $Bi_7O_9I_3$, and $Bi_4O_5I_2$ hierarchical microspheres.

diffusion-controlled processes. There is not enough I^- ion concentration surrounding BiO^+ ions for the formation of BiOI because of diffusion-limited action. Comparatively speaking, there is less I^- ion concentration encircling BiO^+ ions in the glycerol system than that in ethylene glycol because I^- ions have a slower diffusion rate in the former than the latter. On the other hand, according to previous reports, $Bi_7O_9I_3$ and $Bi_4O_5I_2$ have smaller formation energy compared with BiOI.[31] Therefore, $Bi_7O_9I_3$ and $Bi_4O_5I_2$ were preferentially formed in ethylene glycol and glycerol, respectively.

Time-dependent SEM observations were used to study morphological evolution processes of bismuth oxyiodide hierarchical architectures. BiOI was chosen as an example for detailed interpretations. Parts a−c of Figure 4 represent SEM images of the products synthesized with ethanol at 0, 2, and 4 h, respectively. As can be seen from Figure 4a, the products are irregular, small, straight nanosheets before the subsequent alcohothermal reaction. With the reaction time extended to 2 h, these nanosheets became larger and more uniform due to Ostwald ripening. Part of the nanosheets began to assemble into multilayered hierarchical structures (Figure 4b). After 4 h of growth, most of the nanosheest have been assembled into hierarchical architectures (Figure 4c). Upon aging for a longer period up to 12 h, the as-obtained products basically grew into uniform flower-like hierarchical architectures (Figure 2a). The formation processes of hierarchical $Bi_7O_9I_3$ and $Bi_4O_5I_2$ are very similar to that of BiOI except that the initial nanosheets are curly, as shown in Figures S2 and Figure S3 (Supporting Information). The formation of all bismuth oxyiodide hierarchical architectures originated from self-assembly of nanosheets.

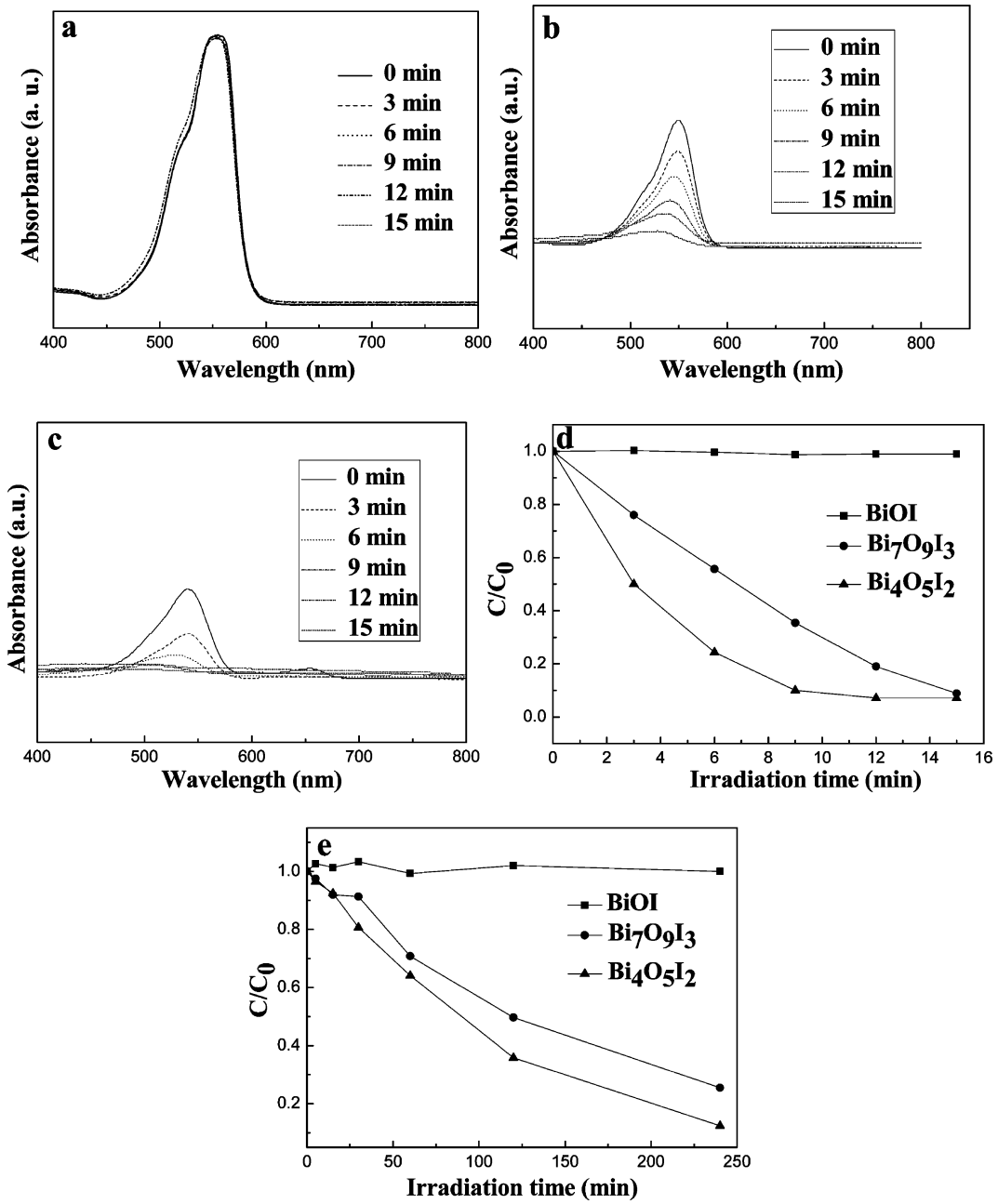

Figure 7. UV−vis absorption spectra changes of RhB aqueous solution in the presence of BiOI (a), $Bi_7O_9I_3$ (b), and $Bi_4O_5I_2$ (c) as a function of irradiation time. The corresponding RhB concentration changes versus irradiation time (d). The phenol concentration changes versus irradiation time (e).

3.4. Surface Areas and Pore Size Distributions. Compared with solid microspheres, the as-obtained bismuth oxyiodide hierarchical architectures fabricated by nanosheets were expected to possess larger specific surface areas and possible hierarchical pore structures. Figure 5 describes typical N_2 adsorption−desorption isotherms and their corresponding pore size distributions for BiOI, $Bi_7O_9I_3$, and $Bi_4O_5I_2$ hierarchical microspheres. BiOI hierarchical microspheres showed a type II adsorption−desorption isotherm, in which the weak adsorption−desorption hysteresis indicated monolayer absorption. However, both $Bi_7O_9I_3$ and $Bi_4O_5I_2$ hierarchical microspheres displayed type IV isotherm character, suggesting the existence of mesopores. The shapes of hysteresis loops for $Bi_7O_9I_3$ and $Bi_4O_5I_2$ hierarchical microspheres resemble type H3, which is associated with slitlike pores.[32] The pore size distribution curves were calculated through the Barrett−Joyner−Halenda method. As shown in Figure 5b, for $Bi_7O_9I_3$ and $Bi_4O_5I_2$ hierarchical microspheres, their pore size distribution curves are quite broad with small mesopores (several nanometers) and larger ones (dozens of nanometers), respectively. The smaller mesopores reflect pores within nanosheets, whereas larger ones can be correlated to the pores formed between stacked nanosheets. Almost no mesopores existed in BiOI hierarchical microspheres. The as-obtained BiOI, $Bi_7O_9I_3$, and $Bi_4O_5I_2$ hierarchical spheres have a BET surface area of 9.7, 35.4, and 66.5 $m^2\ g^{-1}$, respectively.

3.5. Light Absorption and Energy Band Structure. The photocatalytic activity of a semiconductor is closely related to

dx.doi.org/10.1021/am4036702 | ACS Appl. Mater. Interfaces 2013, 5, 11927−11934

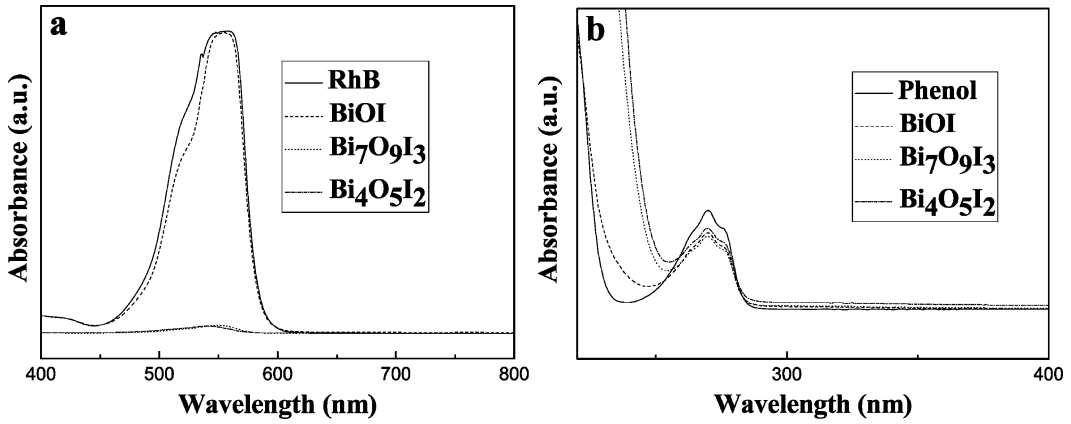

Figure 8. Adsorption behaviors of RhB (a) and phenol (b) on no photocatalysts, and BiOI, $Bi_7O_9I_3$, and $Bi_4O_5I_2$ hierarchical microspheres.

its energy band structure feature. Figure 6a shows the UV−vis DRS spectra of the as-synthesized BiOI, $Bi_7O_9I_3$, and $Bi_4O_5I_2$ hierarchical microspheres, respectively. All of the samples show strong absorption in the UV- and visible-light regions. From BiOI to $Bi_4O_5I_2$ and $Bi_7O_9I_3$, their absorption edge wavelengths are decreasing. The colors of corresponding products, as shown in Figure 6b, gradually lighten, which is in agreement with the results of their UV−vis DRS spectra. The steep absorption edge of the three spectra indicates that their visible-light absorption is not due to the transition from the impurity level but to the band gap transition. BiOI, Bi_7O_9I, and $Bi_4O_5I_2$ are indirect semiconductors, and their band gap energies can be calculated from the plot of $(\alpha h\nu)^{1/2}$ versus photon energy $(h\nu)$. The intercept of the tangent to the x axis will give a good approximation of the band gap energy for hierarchical BiOI, Bi_7O_9I, and $Bi_4O_5I_2$, as shown in Figure 6c. The estimated band gap energies of the as-obtained BiOI, Bi_7O_9I, and $Bi_4O_5I_2$ microspheres were about 1.82, 1.93, and 2.06 eV from the absorption onsets, respectively. The band-edge positions of the as-synthesized bismuth oxyiodide compounds can be calculated by the empirical equation, $E_{VB} = X - E^e + 0.5E_g$, where E_{VB} is the valence band-edge potential, X is the electronegativity of the corresponding semiconductor, expressed as the geometric mean of the absolute electronegativity of the constituent atoms, E^e is the energy of free electrons on the hydrogen scale (ca. 4.5 eV), and E_g is the band gap energy of the semiconductor; E_{CB} can be determined by $E_{CB} = E_{VB} - E_g$.[33] The X values for BiOI, $Bi_7O_9I_3$, and $Bi_4O_5I_2$ are ca. 5.94, 5.93, and 5.93 eV, respectively. The band gap energies of BiOI, $Bi_7O_9I_3$, and $Bi_4O_5I_2$ are 1.82, 2.06, and 1.93 eV, respectively. Given the equation above, the top of the valence band and the bottom of the conduction band of BiOI, $Bi_7O_9I_3$, and $Bi_4O_5I_2$ are calculated to be 2.35 and 0.53 eV, 2.46 and 0.40 eV, and 2.40 and 0.47 eV, respectively.

3.6. Photocatalysis. Selecting RhB and phenol as pollutant models, visible-light-responding photocatalytic activities of BiOI, $Bi_7O_9I_3$, and $Bi_4O_5I_2$ hierarchical architectures were evaluated. Parts a−c of Figure 7 show the temporal evolution of the UV−vis absorption spectra of RhB on BiOI, $Bi_7O_9I_3$, and $Bi_4O_5I_2$ hierarchical microspheres. As can be seen from the above three spectra, the absorbance of RhB in both $Bi_7O_9I_3$ and $Bi_4O_5I_2$ suspensions gradually decreased during the photo-irradiation process. The major absorption peak corresponding to RhB was also shifted from 553 to shorter wavelengths, indicating the removal of ethyl groups one by one.[34] The facts also show that the degradation of RhB results from the combined action of photocatalysis of the semiconductor and photosensitization of RhB. The absorbance of RhB in the BiOI suspension is hardly changed, which shows that the present BiOI hierarchical microspheres have very low photocatalytic activity under the same photocatalytic reaction conditions. The plots for the concentration changes of RhB versus irradiation time over BiOI, $Bi_7O_9I_3$, and $Bi_4O_5I_2$ hierarchical microspheres are shown in Figure 7d. It can be seen that RhB could be quickly decolorized within 15 min in the presence of $Bi_4O_5I_2$, whereas it has negligible degradation on BiOI under the same conditions. $Bi_4O_5I_2$ shows superior photocatalytic activities to $Bi_7O_9I_3$ in decomposing RhB. When colorless phenol was substituted for dye RhB, as shown in Figure 7e, hierarchical BiOI still has very weak photocatalytic activities. However, differently, $Bi_7O_9I_3$ hierarchical microspheres have better photocatalytic activities than $Bi_4O_5I_2$ ones for the degradation of phenol.

The photocatalytic activity of the material in decomposing organic compounds depends on its adsorption ability to reactant, surface area, utilization of the light energy, and energy band-edge potential. Although BiOI hierarchical microspheres can capture most light energy among them, they have extremely poor adsorption ability to RhB (Figure 8a), the least surface area, and the lowest valence potential. Thus, it shows negligible photocatalytic activity in decomposing RhB. Compared with hierarchical $Bi_7O_9I_3$, $Bi_4O_5I_2$ has a smaller valence potential and lower conduction potential. Larger valence potential benefits direct photocatalytic decomposition of RhB, whereas lower conduction potential is helpful for photosensitized degradation processes. On the whole, band-edge potential has a negligible contribution to their difference of photocatalytic activity. As a result, we observed a larger surface area, wider light absorption range, and slightly stronger adsorption ability to RhB of $Bi_4O_5I_2$ hierarchical microspheres than $Bi_7O_9I_3$ ones, which were ascribed to better photocatalytic activity for the former than the latter. The degradation of phenol resulted from the direct photocatalytic process of bismuth oxyiodide hierarchical microspheres. The valence potentials of these bismuth oxyiodide semiconductors play crucial roles in dominating their photocatalytic abilities. They have similar adsorption ability to phenol (Figure 8b). The valence potential from $Bi_7O_9I_3$ to $Bi_4O_5I_2$ and BiOI gradually decreased. As a result, $Bi_7O_9I_3$ showed better photocatalytic activities for the degradation of phenol than $Bi_4O_5I_2$.

3.7. Phosphate Removal. As one of main sources of eutrophication in water, phosphate removal from wastewater

has received great attention.[35] Herein, the as-synthesized $Bi_7O_9I_3$, $Bi_4O_5I_2$, and BiOI hierarchical microspheres were evaluated as adsorbents to remove phosphate from water. Figure 9 represents the adsorption rate of phosphate on these

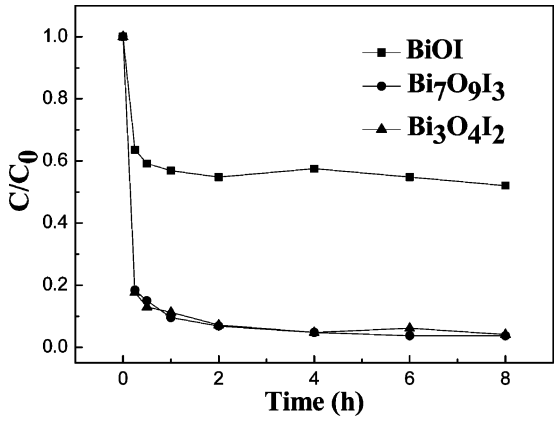

Figure 9. Adsorption rate of phosphate on the as-obtained BiOI, $Bi_7O_9I_3$, and $Bi_4O_5I_2$ hierarchical microspheres.

bismuth oxyiodide hierarchical microspheres obtained by batch tests for an initial phosphate concentration of 10 mg/L at pH = 7. As can be seen from Figure 9, the adsorption rate was rather fast for $Bi_7O_9I_3$ and $Bi_4O_5I_2$ samples. In such experimental conditions, most of the phosphate could be removed after 8 h and the removal capacity of phosphate on $Bi_7O_9I_3$ and $Bi_4O_5I_2$ samples was measured to be ca. 48.1 and 48.0 mg g^{-1}, respectively, which is comparable to mesoporous spheres containing iron and aluminum oxide,[36] mesoporous silica MCM-41 containing aluminum,[37] and $LaPO_4$ modified nanoporous SBA-15.[38] The good adsorption performance for $Bi_7O_9I_3$ and $Bi_4O_5I_2$ microspheres can be ascribed to their larger surface area and hierarchical porous structures.

4. CONCLUSIONS

In summary, hierarchical BiOI, $Bi_7O_9I_3$, and $Bi_4O_5I_2$ microspheres assembled by nanosheets have been synthesized on a large scale through selecting ethanol, ethylene glycol, and glycerol as solvents, respectively. The formation of $Bi_7O_9I_3$ and $Bi_4O_5I_2$ obeyed the diffusion-limited process because of the larger viscosity of ethylene glycol and glycerol. The as-obtained hierarchical BiOI, $Bi_7O_9I_3$, and $Bi_4O_5I_2$ microspheres showed different surface areas, light absorption ranges, and energy band structures. When they were used as visible-light-driven photocatalysts, BiOI microspheres showed the lowest photocatalytic activities in degradation of both RhB and phenol. $Bi_4O_5I_2$ microspheres had the best photocatalytic activities in decomposing of RhB, whereas $Bi_7O_9I_3$ ones showed the best photocatalytic activities for the degradation of phenol among them. On the basis of the adsorption ability to reactant, surface area, utilization of the light energy, and energy band-edge potentials of BiOI, $Bi_7O_9I_3$, and $Bi_4O_5I_2$ hierarchical microspheres, the difference of their photocatalytic activities was discussed. In addition, when evaluated as adsorbents to remove phosphate from water, hierarchical $Bi_7O_9I_3$ and $Bi_4O_5I_2$ microspheres showed good adsorption abilities. The present study provides some important information on relative photocatalytic activities of bismuth oxyiodide compounds. The as-synthesized $Bi_7O_9I_3$ and $Bi_4O_5I_2$ hierarchical spheres with good photocatalytic activities and adsorption abilities for phosphate in water are potentially applicable in the field of environmental remediation.

■ ASSOCIATED CONTENT

Supporting Information

EDX spectra of BiOI, $Bi_7O_9I_3$, and $Bi_4O_5I_2$ hierarchical microspheres and FE-SEM images of the products synthesized at different reaction stages. This material is available free of charge via the Internet at http://pubs.acs.org.

■ AUTHOR INFORMATION

Corresponding Authors

*E-mail: dkma@wzu.edu.cn. Fax: +86-577-8837-3017. Tel: +86-577-8837-3031.
*E-mail: smhuang@wzu.edu.cn.

Notes

The authors declare no competing financial interest.

■ ACKNOWLEDGMENTS

We would like to acknowledge the partial financial support from the NSFC (51002107, 51372173, and 21173159), NSFC for Distinguished Young Scholars (51025207), ZJSTD Key Innovative Team (2012R10014-07), and ZJED Innovative Team for S.-M. Huang.

■ REFERENCES

(1) Venkataramanan, N. S.; Matsui, K.; Kawanami, H.; Ikushima, Y. *Green Chem.* **2007**, *9*, 18−19.
(2) Fernandez, C. A.; Bekhazi, J. G.; Hoppes, E. M.; Wiacek, R. J.; Fryxell, G. E.; Bays, J. T.; Warner, M. G.; Wang, C. M.; Hutchison, J. E.; Addleman, R. S. *Small* **2009**, *5*, 961−969.
(3) Johnson, J. M.; Kinsinger, N.; Sun, C. H.; Li, D. S.; Kisailus, D. *J. Am. Chem. Soc.* **2012**, *134*, 13974−13977.
(4) Linley, S.; Leshuk, T.; Gu, F. X. *ACS Appl. Mater. Interfaces* **2013**, *5*, 2540−2548.
(5) Lei, W. W.; Portehault, D.; Liu, D.; Qin, S.; Chen, Y. *Nat. Commun.* **2013**, *4*, 1777.
(6) Du, J.; Pan, Y. D.; Zhang, T. R.; Han, X. P.; Cheng, F. Y.; Chen, J. *J. Mater. Chem.* **2012**, *22*, 15812−15818.
(7) Wang, Y. L.; Xia, Y. N. *Nano Lett.* **2004**, *4*, 2047−2050.
(8) Liu, Z. P.; Peng, S.; Xie, Q.; Hu, Z. K.; Yang, Y.; Zhang, S. Y.; Qian, Y. T. *Adv. Mater.* **2003**, *15*, 936−940.
(9) Chen, C. C.; Ma, W. H.; Zhao, J. C. *Chem. Soc. Rev.* **2010**, *39*, 4206−4219.
(10) Abbaspourrad, A.; Carroll, N. J.; Kim, S. H.; Weitz, D. A. *Adv. Mater.* **2013**, *25*, 3215−3221.
(11) Zhang, N.; Ouyang, S. X.; Kako, T.; Ye, J. H. *Chem. Commun.* **2012**, *48*, 9894−9896.
(12) Li, G. S.; Jiang, B.; Li, X.; Lian, Z. C.; Xiao, S. N.; Zhu, J.; Zhang, D. Q.; Li, H. X. *ACS Appl. Mater. Interfaces* **2013**, *5*, 7190−7197.
(13) Zhou, H.; Li, X. F.; Fan, T. X.; Osterloh, F. E.; Ding, J.; Sabio, E. M.; Zhang, D.; Guo, Q. X. *Adv. Mater.* **2010**, *22*, 951−956.
(14) Zhong, L. S.; Hu, J. S.; Cao, A. M.; Liu, Q.; Song, W. G.; Wan, L. J. *Chem. Mater.* **2007**, *19*, 1648−1655.
(15) Hu, J. S.; Zhong, L. S.; Song, W. G.; Wan, L. J. *Adv. Mater.* **2008**, *20*, 2977−2982.
(16) Zhou, J. B.; Yang, S. L.; Yu, J. G.; Shu, Z. *J. Hazard. Mater.* **2011**, *192*, 1114−1121.
(17) Ma, D. K.; Huang, S. M.; Chen, W. X.; Hu, S. W.; Shi, F. F.; Fan, K. L. *J. Phys. Chem. C* **2009**, *113*, 4369−4374.
(18) Zhang, Z. P.; Sun, H. P.; Shao, X. Q.; Li, D. F.; Yu, H. D.; Han, M. Y. *Adv. Mater.* **2005**, *17*, 42−47.
(19) Zhu, J. J.; Xu, S.; Wang, H.; Zhu, J. M.; Chen, H. Y. *Adv. Mater.* **2003**, *15*, 156−159.
(20) Zhang, T. R.; Dong, W. J.; Keeter-Brewer, M.; Konar, S.; Njabon, R. N.; Tian, Z. R. *J. Am. Chem. Soc.* **2006**, *128*, 10960−10968.

(21) Ma, D. K.; Jiang, J. L.; Huang, J. R.; Yang, D. P.; Cai, P.; Zhang, L. J.; Huang, S. M. *Chem. Commun.* **2010**, *46*, 4556−4558.
(22) Ma, D. K.; Zhou, S. M.; Hu, X.; Jiang, Q. R.; Huang, S. M. *Mater. Chem. Phys.* **2013**, *140*, 11−15.
(23) Jiang, J.; Zhao, K.; Xiao, X. Y.; Zhang, L. Z. *J. Am. Chem. Soc.* **2012**, *134*, 4473−4476.
(24) Xiao, X.; Zhang, W. D. *RSC Adv.* **2011**, *1*, 1099−1105.
(25) Ye, L. Q.; Tian, L. H.; Peng, T. Y.; Zan, L. *J. Mater. Chem.* **2011**, *21*, 12479−12484.
(26) Xia, J. X.; Yin, S.; Li, H. M.; Xu, H.; Yan, Y. S.; Zhang, Q. *Langmuir* **2011**, *27*, 1200−1206.
(27) Hahn, N. T.; Hoang, S.; Self, J. L.; Mullins, C. B. *ACS Nano* **2012**, *6*, 7712−7722.
(28) Ye, L. Q.; Chen, J. N.; Tian, L. H.; Liu, J. Y.; Peng, T. Y.; Deng, K. J.; Zan, L. *Appl. Catal., B* **2013**, *130*, 1−7.
(29) Xiao, X.; Liu, C.; Hu, R. P.; Zuo, X. X.; Nan, J. M.; Li, L. S.; Wang, L. S. *J. Mater. Chem.* **2012**, *22*, 22840−22843.
(30) Schmidt, M.; Oppermann, H.; Briickner, H.; Binnewies, M. *Z. Anorg. Allg. Chem.* **1997**, *623*, 1945−1953.
(31) Rittner, P.; Oppermann, H. *Z. Anorg. Allg. Chem.* **1992**, *617*, 131−135.
(32) Sing, K. S. W.; Everett, D. H.; Haul, R. A. W.; Moscou, L.; Pierotti, R. A.; Rouquerol, J.; Siemieniewska, T. *Pure Appl. Chem.* **1985**, *57*, 603−619.
(33) Guan, M. L.; Ma, D. K.; Hu, S. W.; Chen, Y. J.; Huang, S. M. *Inorg. Chem.* **2011**, *50*, 800−805.
(34) Fu, H. B; Pan, C. S.; Yao, W. Q.; Zhu, Y. F. *J. Phys. Chem. B* **2005**, *109*, 22432−22439.
(35) Emmanuelawati, I.; Yang, J.; Zhang, J.; Zhang, H. W.; Zhou, L.; Yu, C. Z. *Nanoscale* **2013**, *5*, 6173−6180.
(36) de Sousa, A. F.; Braga, T. P.; Gomes, E. C. C.; Valentini, A.; Longhinotti, E. *Chem. Eng. J.* **2012**, *210*, 143−149.
(37) Li, D. D.; Min, H. Y.; Jiang, X.; Ran, X. Q.; Zou, L. Y.; Fan, J. W. *J. Colloid Interface Sci.* **2013**, *404*, 42−48.
(38) Yang, J.; Zhou, L.; Zhao, L. Z.; Zhang, H. W.; Yin, J. N.; Wei, G. F.; Qian, K.; Wang, Y. H.; Yu, C. Z. *J. Mater. Chem.* **2011**, *21*, 2489−2494.